



## Integrated process for partial oxidation of heavy oil and in-situ reduction of red mud

Dechao Wang, Yang Li, Lijun Jin, Kaihui Hao, Baoyong Wei, Demeng Yao, Haoquan Hu\*

*State Key Laboratory of Fine Chemistry, Institute of Coal Chemical Engineering, School of Chemical Engineering, Dalian University of Technology, Dalian 116024, China*



### ARTICLE INFO

**Keywords:**

Heavy oil  
Upgrading  
Red mud  
Coke  
Partial oxidation  
Chemical looping

### ABSTRACT

RM was used for the upgrading of vacuum residue (VR) by partial oxidation (POX). The function of diverse metal oxides in RM during VR upgrading was clarified and the utilization of used RM was developed. The results show that POX of VR with RM600 (calcined RM at 600 °C) decreases the cracking temperature, and increases heavy oil conversion and light fuels yield. The active sites Fe and O are highly dispersed on RM600, and Na species doping results in the formation of sodium ferrite, creating oxygen vacancy. Large specific surface area is remained after reaction due to the presence of Al<sub>2</sub>O<sub>3</sub>, SiO<sub>2</sub> and TiO<sub>2</sub>. Fe<sub>2</sub>O<sub>3</sub> in RM600 is in-situ reduced to Fe<sub>3</sub>O<sub>4</sub>, which could be further reduced by deposited coke on spent RM600 to produce Fe. The spent RM600 could be reused through a chemical looping POX and the yield of light fuels remains stable during 20 cycles.

### 1. Introduction

The unconventional oil resources such as heavy oil, extra-heavy oil, and bitumen is about 70% of the world's total oil reserves [1]. Processing unconventional oil produces a large amount of residual oil, including atmospheric and vacuum residue. Modern refineries incorporate unites for heavy oil upgrading on the basis of thermal or catalytic conversion routes [1]. Among these, POX process is considered as an alternative technology for heavy oil upgrading. This process has been reported for producing syngas from methane [2,3] or light fuels from heavy oil [4]. Compared to typical thermal cracking process, high heavy oil conversion and light fuels yield can be achieved by POX [5]. Generally, the operating conditions of POX are usually conducted at the temperature range of 450–550 °C and atmospheric pressure [6,7]. The choice of oxidants is one of the important factors for the development of POX process. Several oxidants including O<sub>2</sub> [8], H<sub>2</sub>O [9], H<sub>2</sub>O<sub>2</sub> [10], and transition metal oxides [11] have been used for heavy oil upgrading. Among transition metal oxides, the use of iron oxide based materials has received much attention due to its high activity, environmental friendly nature, and low price [5,12]. The role of iron oxide in heavy oil upgrading is to provide active oxygen species ([O]). As a result, more heavy oil are converted into light fuels and the [O] is mainly converted to CO or CO<sub>2</sub> [11].

Red mud (RM), a reddish-brown caustic solid waste residue, is the byproduct of alumina production [13]. The average production of 1.0 ton of alumina can produce 0.5–2.0 ton of RM, and the annual

global RM production is about 120 million tons [14]. When RM is produced, it is usually pumped into holding ponds [15]. However, there are many problems with managing RM including costly maintenance of RM pond, waste of land resource, risk of caustic pollutants for all living organisms, and leakage of alkaline contaminants into groundwater resources [16]. RM consists of a diverse of mixed metal oxides, including Fe<sub>2</sub>O<sub>3</sub>, Al<sub>2</sub>O<sub>3</sub>, TiO<sub>2</sub>, SiO<sub>2</sub>, CaO, and Na<sub>2</sub>O as well as some trace elements [13]. Generally, Fe<sub>2</sub>O<sub>3</sub> is the main component of RM, usually from 30 to 60% [14]. Other iron oxides including hydroxide (Fe(OH)<sub>3</sub>), goethite (FeOOH), magnetite (Fe<sub>3</sub>O<sub>4</sub>) are also present in the RM [17]. The substitution of RM to commercial catalysts can reduce the cost related to the use of commercial catalysts and avoid the pollution hazard caused by the disposal of RM [18,19]. Jahromi and Agblevor prepared RM supported nickel catalysts at different concentrations of nickel and applied for hydro-deoxygenated pinyon-juniper catalytic pyrolysis oil [18]. Weber et al. investigated the conversion of key oxygenates in fast pyrolysis oil to produce high value chemicals with greater energy density and stability over reduced RM [20]. Mendonça et al. reported that thermal treatment of the bio-oil aqueous acid fraction over RM at the temperature range of 400–800 °C could produce a solid composite, including Fe and carbon [21]. Moreover, RM shows application in heavy oil upgrading. Nguyen-Huy and Shin synthesized ZrO<sub>2</sub>-impregnated macro-mesoporous RM catalysts and applied for the POX of VR under a steam atmosphere [6]. Lee et al. found that 3 wt% ZrO<sub>2</sub>-impregnated RM exhibited the best POX performance of VR due to the largest specific surface area and high catalyst stability [7]. However,

\* Corresponding author.

E-mail address: [hhu@dlut.edu.cn](mailto:hhu@dlut.edu.cn) (H. Hu).

the function of diverse main components in RM in POX of heavy oil remains to be elucidated.

When RM was used for the catalytic pyrolysis of plastic waste, the CO<sub>2</sub> yield increases due to the incorporation of [O] on Fe<sub>2</sub>O<sub>3</sub> [22]. The supply of [O] causes the crystal transition from hematite (Fe<sub>2</sub>O<sub>3</sub>) to magnetite (Fe<sub>3</sub>O<sub>4</sub>), resulting in the deactivation of catalyst [7]. If spent RM is directly discarded, it is easy to cause secondary pollution. Therefore, the development of new technology for the conversion of spent RM into useful products will be the final fate of RM residue. On the one hand, the decomposition of heavy oil will generate coke, which is deposited on the spent RM. The use of coke as a reductant can further reduce the Fe<sub>3</sub>O<sub>4</sub> to produce FeO or metallic Fe, providing a new method for recovery of useful metal from solid waste. On the other hand, the spent RM can be recycled and used for POX of heavy oil. When the spent RM is treated under air condition, the consumed [O] is replenished and coke is burnt off. The regenerated RM can be reused for the heavy oil upgrading, completing the redox cycle. This process is referred as chemical looping (CL), which usually consists of two reactors, including fuel and air reactor. The metal oxide is circulated between the reactors to release and store oxygen. CL has been applied for steam reforming for high purity hydrogen production [23], dehydrogenation of ethane for ethylene [24], and methane dry reforming [25] and partial oxidation for syngas production [26]. In our previous work, a CL partial oxidation (CLPOX) was proposed for the heavy oil upgrading by using iron-based metal oxides as oxygen carrier [5]. As a result, the yield of light fuels such as gasoline, diesel remains stable after several cycles.

To address the above issues, we proposed a process to integrate POX of heavy oil and in-situ reduction of Fe<sub>2</sub>O<sub>3</sub> in RM. Petroleum residue, VR, was used as feedstock. The POX performance was conducted on thermogravimetric (TG) and fixed bed reactor to obtain weight loss behavior and products distribution, respectively. The role of diverse compositions in upgrading of heavy oil was clarified by means of various characterization methods. New technologies for the utilization of spent RM were studied. The spent RM600 (sRM600) was treated under N<sub>2</sub> atmosphere to produce useful metallic Fe and several characterizations were performed to reveal the change of Fe species. In addition, the CLPOX performance of RM600 with the aim for stable light fuels production was also conducted.

## 2. Experimental

### 2.1. Pretreatment of RM

RM sample is from CHALCO Shandong CO., LTD (Shandong province, China). The chemical composition of RM is shown in Table 1. The main component in RM is Fe<sub>2</sub>O<sub>3</sub> with content of 39.0 wt%, followed by SiO<sub>2</sub> and Al<sub>2</sub>O<sub>3</sub> being 22.2 wt% and 21.4 wt%, respectively. The raw RM was dried at 110 °C for 24 h and subsequently calcined at 600 °C for 3 h (denoted as RM600) before being used for POX.

### 2.2. Partial oxidation

VR is from PetroChina Fushun Petrochemical Company and its basic properties and elemental analysis are shown in Table 2. During each test, feedstock with 20 wt% VR in toluene was used. In TG analysis, RM600 was added into VR solution under mechanical stirring at 30 °C for 2 h to ensure an intimate contact between VR and RM. After that,

**Table 1**  
Chemical composition of RM determined by XRF.

Component	Fe <sub>2</sub> O <sub>3</sub>	SiO <sub>2</sub>	Al <sub>2</sub> O <sub>3</sub>	Na <sub>2</sub> O	TiO <sub>2</sub>	CaO	K <sub>2</sub> O	Other <sup>a</sup>
Content (wt%)	39.0	22.2	21.4	11.3	3.6	1.5	0.2	0.8

\* By difference.

**Table 2**  
Properties of VR.

Mn <sup>a</sup>	> 500 °C fraction (wt%)	Elemental analysis (wt%)				
		C	H	N	S + O <sup>b</sup>	H/C
1061	86.5	86.34	12.92	0.57	0.17	1.80

<sup>a</sup> Number-average molecular weight.

<sup>b</sup> By difference.

the mixture was heated at 80 °C under vacuum condition for 24 h to remove toluene. The mass ratio of VR to RM600 is 0.8. For comparison, blank test by using SiO<sub>2</sub> was carried out. TG (Mettler Toledo, SDTA851<sup>e</sup>) analysis was performed to investigate the weight change with respect to temperature. About 15 mg sample was heated from 25 to 700 °C with a heating rate of 10 °C/min, and the flow rate of N<sub>2</sub> is 60 mL/min.

Although TG analysis is able to obtain the weight change with temperature, it is difficult to collect and analyze the final products. Moreover, RM samples before and after reaction are needed to be characterized to understand the function of each components. Therefore, POX of VR was performed on a fixed bed reactor to collect and analyze the cracking products. Detail description of POX of VR can be found elsewhere [11,27]. POX was performed at 550 °C for 1 h under atmospheric pressure as shown in Fig. S1. The weight hourly space velocity (WHSV, the mass ratio of between VR and RM600/SiO<sub>2</sub>) is 0.8 h<sup>-1</sup>. The liquid and gas products were collected and analyzed. Oil fraction distribution was determined by simulated distillation on a SCION 456-GC equipped with a CP-SimDist column (10 m × 0.53 mm × 0.88 μm). According to the boiling point, it can be classified as gasoline (IPB-180 °C), diesel (180–350 °C), vacuum gas oil (VGO, 350–500 °C) and heavy oil (> 500 °C) [1,11]. Chemical compositions of liquid product were identified on a GC (Agilent 7890A) coupled to a mass spectrometry detector (GC/MS) with a scan mass range of *m/z* 50–550. The composition in gas was analyzed on a GC 7890 II.

### 2.3. Characterization

XRD patterns were recorded on a D/Max 2400 diffractometer. Textural properties were measured by N<sub>2</sub> adsorption-desorption isotherms at 77 K on a JK-BK 122 W. The specific surface area was calculated by Brunauer-Emmett-Teller (BET) method. SEM morphology was recorded on QUANTA 450. The amount of coke deposited on sRM600 was determined on Mettler Toledo TGA/SDTA851<sup>e</sup> from 25 to 850 °C with a heating rate of 10 °C/min. The air flow rate is 60 mL/min. XPS analysis was conducted on a Thermo Scientific<sup>TM</sup> ESCALAB 250Xi spectrometer with a monochromatic Al K $\alpha$  radiation (150 W, 1486.6 eV) for analysis of the core level signal of Fe 2p. The binding energy was corrected to C1s peak (284.8 eV) to account for charging effects. Raman spectra was measured on a Thermo Fisher DXR Microscope. H<sub>2</sub> temperature programmed reduction (H<sub>2</sub>-TPR) experiments were carried out in a U-tube quartz reactor under H<sub>2</sub> atmosphere from 200 °C to 900 °C with a heating rate of 5 °C/min. The room temperature <sup>57</sup>Fe Mössbauer spectra were obtained on a Topologic 500A spectrometer with a proportional counter. The <sup>57</sup>Co(Rh) source in a constant acceleration mode was used as γ-ray radioactive source.

## 3. Results and discussion

### 3.1. Partial oxidation of VR

The total weight of VR decreases with the increase of temperature as shown in Fig. 1. At low temperature, weight loss is mainly due to the distillation of hydrocarbon molecules with low boiling point and the

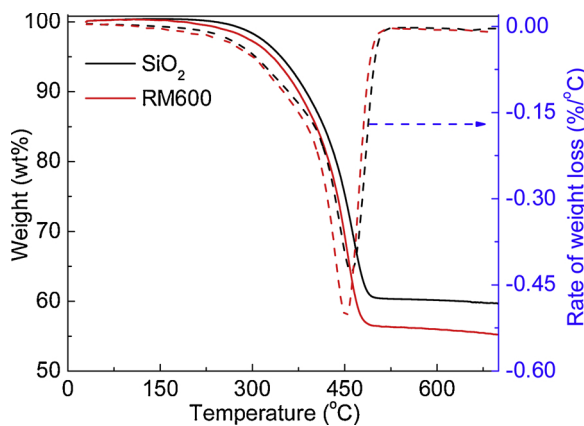


Fig. 1. TG and DTG curves of VR over RM600 and  $\text{SiO}_2$ .

cleavage of weak chemical bonds [28]. The largest weight loss is in the temperature range of 300–500 °C. It is related to complex reactions such as the cleavage of C-C and C-heteroatom bonds in the alkanes and alkyl side chains attached to naphthenic or aromatic rings, the dehydrogenation and ring-opening of naphthenic rings, and the dehydrogenation of the aromatic ring structure [28]. As shown in Fig. 1, the weight loss behavior over  $\text{SiO}_2$  and RM600 are different. In the case of  $\text{SiO}_2$ , the weight loss appears at 210 °C, peak of the maximum weight loss rate is around 460 °C, and the total weight loss is 40.4 wt%. For RM600, the corresponding temperature decreases to 180 °C and 450 °C, respectively, and the final total weight loss increases to 44.7 wt%. Fig. S2 shows that the addition of  $\text{Fe}_2\text{O}_3$  is also contributed to the cracking of VR. It has been reported that  $\text{Fe}_2\text{O}_3$  in RM is the active sites to offer the [O] to react with heavy oil [11]. As a result, the presence of  $\text{Fe}_2\text{O}_3$  in RM results in the decrease of cracking temperature and the increase of total weight loss.

With the help of TG, different cracking behavior of VR over RM600 and  $\text{SiO}_2$  can be noted, but the products distribution cannot be quantitatively obtained. POX of VR was then performed on a fixed bed reactor to obtain products distribution as shown in Table 3. The thermal cracking of heavy oil follows a free radical mechanism, where cracking reactions are the initial step, and the condensation and polymerization reactions are the final step [29]. The former results in the production of light fuels, and the latter explains the formation of carbonaceous residue (CR). In this case, the yields of gas, gasoline, diesel, and VGO are 3.0, 6.6, 14.6, and 20.1 wt%, respectively. Heavy oil is converted in CR with yield of 27.5 wt%, which indicates an invalid conversion of heavy oil over  $\text{SiO}_2$ . For RM600, heavy oil conversion increases from 67.5 wt % to 96.3 wt%. The yields of gas, gasoline, diesel and VGO are 6.8, 10.3, 38.0, and 27.7 wt%, respectively, while CR yield decreases to 14.0 wt%. Compared with  $\text{SiO}_2$ , the increase in gas, gasoline, diesel and VGO yields on RM600 is mainly attributed to a deep heavy oil conversion and decrease in CR. The elemental composition of upgraded oil is shown in Table S1. It can be seen that upgraded oil from thermal cracking or POX shows a higher H/C ratio as compared to raw VR. Moreover, the H/C ratio on RM600 is 1.89, higher than that on  $\text{SiO}_2$  (1.84).

Table 3  
Products distribution and heavy oil conversion from POX of VR.

Sample	Yield (wt%)					Heavy oil conversion <sup>*</sup> (wt%)
	Gasoline	Diesel	VGO	Gas	CR	
$\text{SiO}_2$	6.6	14.6	20.1	3.0	27.5	67.5
RM600	10.3	38.0	27.7	6.8	14.0	96.3

\* Heavy oil conversion = (1-heavy oil in liquid product/heavy oil in VR) × 100%.

Table 4  
Composition of gas from POX of VR.

Sample	Gas composition (vol%)						
	$\text{CO}_2$	$\text{CH}_4$	$\text{C}_2\text{H}_4$	$\text{C}_2\text{H}_6$	$\text{C}_3\text{H}_8$	$\text{H}_2$	CO
$\text{SiO}_2$	0.5	36.1	22.6	17.4	10.1	13.3	*
RM600	3.1	10.9	6.6	4.2	2.8	68.1	4.3

\* Undetected by GC.

As shown in Table 4, composition of gas from thermal cracking mainly includes hydrocarbon molecules, of which methane shows the highest content being 36.1 vol%. The formation of  $\text{CH}_4$  below 650 °C is due to the cleavage of alkyl chains, cycloalkanes, and alky side chains attached to aromatic rings and naphthenic rings [30]. The  $\text{CH}_3$  radical is stabilized by H radical to form  $\text{CH}_4$  [30,31]. The formation of  $\text{CO}_2$  is associated with the decomposition of carboxyl functional groups [30], but its content is only 0.5 vol% on  $\text{SiO}_2$ . With the addition of RM600, the content of  $\text{CH}_4$  decreases from 36.1 to 10.9 vol%, while the  $\text{H}_2$  content increases from 12.7 to 68.1 vol%. It should be noted that the  $\text{CO}_2$  content increases from 0.5 to 3.1 vol%. A high proportion of  $\text{CO}_2$  was also noted when RM was used for catalytic pyrolysis of plastic wastes [22]. In this case, the formation of  $\text{CO}_2$  is mainly attributed to the stepwise reduction of  $\text{Fe}_2\text{O}_3$  in RM to form reduced iron oxide by the reaction between hydrocarbon molecules and [O] in  $\text{Fe}_2\text{O}_3$  [22]. The content of CO is 4.3 vol% on RM600. Thus, the formation of CO and  $\text{CO}_2$  is also due to the stepwise reduction of  $\text{Fe}_2\text{O}_3$  in RM.

The results from Table 3 show that the addition of RM600 increases the yields of gasoline, diesel and VGO, and decreases the yield of CR. The GC/MS analysis was performed to determine chemical compounds and their relative content. Fig. S3a shows the total ion chromatogram of the upgraded oil from POX of VR on RM600. The multiple peaks suggest the complex of upgraded oil. With the increase of retention time, peak intensity decreases, indicating the decrease in relative content. The identified chemical compounds and their relative content are shown in Table 5. The resulting liquid mainly contains alkanes and alkenes. As shown in Fig. S3b and Table S2, the VR toluene-soluble fraction contains long straight-chain alkanes. After POX, the content of these long straight-chain alkanes decreases, while the content of short chain alkanes and alkenes increases significantly. This indicates that the addition of RM600 contributes to the cracking of long straight-chain alkane. The above results show that RM is a good oxidant that can be used for the POX of heavy oil for producing light fuels.

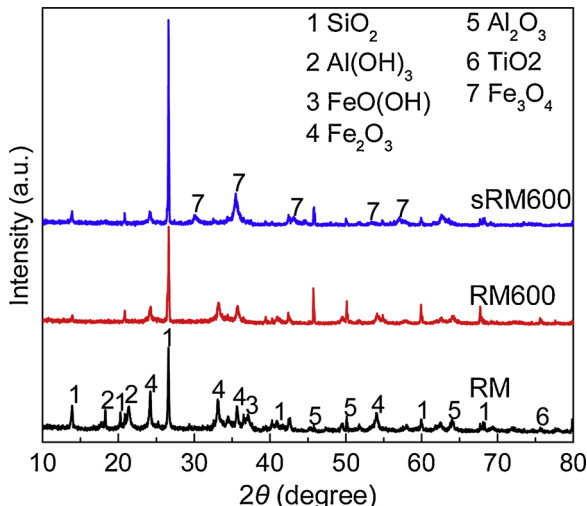
### 3.2. Characterization of RM

As shown in Table 4, a significant increase in  $\text{CO}_2$  and CO can be noted on RM600, indicating the participation reaction of [O] on RM600. Thus, XRD analysis was conducted to elucidate the crystal phase transition of RM before and after reaction. As shown in Fig. 2, raw RM mainly contains hematite ( $\text{Fe}_2\text{O}_3$ ), quartz ( $\text{SiO}_2$ ), goethite ( $\text{FeOOH}$ ), gibbsite ( $\text{Al}(\text{OH})_3$ ), aluminum oxide ( $\text{Al}_2\text{O}_3$ ), and rutile ( $\text{TiO}_2$ ). As RM contains complex metal oxides, it is possible that diffraction peaks associated with other components are not detected due to highly dispersion of these phases or overlapping [32]. As for RM600, the diffraction peaks assigned to hematite ( $\text{Fe}_2\text{O}_3$ ), quartz ( $\text{SiO}_2$ ), aluminum oxide ( $\text{Al}_2\text{O}_3$ ), and rutile ( $\text{TiO}_2$ ) can still be identified, while peaks corresponding to  $\text{FeOOH}$  and  $\text{Al}(\text{OH})_3$  disappear. The disappearance of  $\text{FeOOH}$  and  $\text{Al}(\text{OH})_3$  is due to the dehydration decomposition of  $\text{FeOOH}$  and  $\text{Al}(\text{OH})_3$  to form  $\text{Fe}_2\text{O}_3$  and  $\text{Al}_2\text{O}_3$ . For sRM600, the diffraction peaks assigned to magnetite ( $\text{Fe}_3\text{O}_4$ ) can be noted, while no peaks attributed to hematite ( $\text{Fe}_2\text{O}_3$ ) are observed. The disappearance of  $\text{Fe}_2\text{O}_3$  and emergence of  $\text{Fe}_3\text{O}_4$  indicate that  $\text{Fe}_2\text{O}_3$  in RM is converted into  $\text{Fe}_3\text{O}_4$ .  $\text{Fe}_2\text{O}_3$  can be considered as oxidant to provide [O] to participate into cracking reaction of heavy oil. The cracking of

**Table 5**

GC/MS identified compounds in the liquid product from POX of VR on RM600.

No.	Compound	Formula	Relative content, %	No.	Compound	Formula	Relative content, %
1	1-Nonene	C <sub>9</sub> H <sub>18</sub>	3.75	2	Nonane	C <sub>9</sub> H <sub>20</sub>	2.04
3	1-Decene	C <sub>10</sub> H <sub>20</sub>	4.71	4	Decane	C <sub>10</sub> H <sub>22</sub>	1.88
5	1-Undecene	C <sub>11</sub> H <sub>22</sub>	3.88	6	Undecane	C <sub>11</sub> H <sub>24</sub>	2.05
7	1-Dodecene	C <sub>12</sub> H <sub>24</sub>	3.14	8	Dodecane	C <sub>12</sub> H <sub>26</sub>	2.22
9	1-Tridecene	C <sub>13</sub> H <sub>26</sub>	2.96	10	Tridecane	C <sub>13</sub> H <sub>28</sub>	1.84
11	1-Tetradecene	C <sub>14</sub> H <sub>28</sub>	3.00	12	Tetradecane	C <sub>14</sub> H <sub>30</sub>	2.29
13	1-Pentadecene	C <sub>15</sub> H <sub>30</sub>	2.60	14	Pentadecane	C <sub>15</sub> H <sub>32</sub>	1.83
15	Benzene, 1,1'-(1,2-ethanediyl)bis-	C <sub>14</sub> H <sub>14</sub>	3.97	16	1-Hexadecene	C <sub>16</sub> H <sub>32</sub>	2.34
17	Hexadecane	C <sub>16</sub> H <sub>34</sub>	1.72	18	1-Heptadecene	C <sub>17</sub> H <sub>34</sub>	2.24
19	Heptadecane	C <sub>17</sub> H <sub>36</sub>	1.90	20	1-Octadecene	C <sub>18</sub> H <sub>36</sub>	2.01
21	Octadecane	C <sub>18</sub> H <sub>38</sub>	1.69	22	1-Nonadecene	C <sub>19</sub> H <sub>38</sub>	1.86
23	Nonadecane	C <sub>19</sub> H <sub>40</sub>	1.72	24	1-Eicosene	C <sub>20</sub> H <sub>40</sub>	1.76
25	Eicosane	C <sub>20</sub> H <sub>42</sub>	1.61	26	1-Heneicosene	C <sub>21</sub> H <sub>42</sub>	1.43
27	Heneicosane	C <sub>21</sub> H <sub>44</sub>	1.46	28	1-Docosene	C <sub>22</sub> H <sub>44</sub>	1.17
29	Docosane	C <sub>22</sub> H <sub>46</sub>	1.36	30	1-Tricosene	C <sub>23</sub> H <sub>46</sub>	0.95
31	Tricosane	C <sub>23</sub> H <sub>48</sub>	1.25	32	1-Tetracosene	C <sub>24</sub> H <sub>48</sub>	0.75
33	Tetracosane	C <sub>24</sub> H <sub>50</sub>	1.04	34	1-Pentacosene	C <sub>25</sub> H <sub>50</sub>	0.66
35	Pentacosane	C <sub>25</sub> H <sub>52</sub>	1.14	36	Hexacosane	C <sub>26</sub> H <sub>54</sub>	0.89
37	Heptacosane	C <sub>27</sub> H <sub>56</sub>	0.77	38	Octacosane	C <sub>28</sub> H <sub>58</sub>	1.02

**Fig. 2.** XRD patterns of RM600, sRM600, and RM.

VR over RM is a POX process because heavy oil is mostly converted to valuable liquid (76.0 wt%). It also should be noted that [O] in Fe<sub>2</sub>O<sub>3</sub> can also react with CR precursors. As a result, the CR yield decreases from 27.5 wt% to 14.0 wt%, and CO<sub>2</sub> and CO increase.

Fig. S4 shows the N<sub>2</sub> adsorption/desorption isotherms of RM, RM600 and sRM600. All isotherms are of type IV, characteristic of mesoporous materials. The hysteresis loops are identified as type H4, which could be associated with capillary condensation, suggesting that pore structure in all the samples is irregular. As shown in Table 6, the specific surface area and pore volume on RM are 18.8 m<sup>2</sup>/g and 0.085 cm<sup>3</sup>/g, respectively. When RM was calcined at 600 °C, the specific surface area and pore volume increase to 30.7 m<sup>2</sup>/g and 0.107 cm<sup>3</sup>/g, respectively. The calcination of RM results in the dehydration decomposition of Al(OH)<sub>3</sub> and FeO(OH) to form Al<sub>2</sub>O<sub>3</sub> and Fe<sub>2</sub>O<sub>3</sub> with the generation of H<sub>2</sub>O. The generation of H<sub>2</sub>O promotes the formation of pore structure. However, the specific surface area and pore

volume of sRM600 decrease to 13.0 m<sup>2</sup>/g and 0.059 cm<sup>3</sup>/g, respectively, which is mainly due to the coke deposition.

To understand chemical state change, XPS spectra of Fe 2p and O 1s of RM600 and sRM600 were recorded and shown in Fig. 3a. Generally, peak positions of satellite, Fe 2p<sub>1/2</sub> and Fe 2p<sub>3/2</sub>, are very sensitive to iron oxidation state, thus, these peaks can be used for determining ionic state of iron [33]. As shown in Fig. 3a, three distinct peaks including Fe 2p<sub>1/2</sub> (724.5 eV), satellite peak (718.9 eV), and Fe 2p<sub>3/2</sub> (710.9 eV) can be noted on RM600, corresponding to Fe<sup>3+</sup> in Fe<sub>2</sub>O<sub>3</sub> [34]. Peaks of Fe 2p<sub>1/2</sub> and Fe 2p<sub>3/2</sub> are located at 724.2 eV and 710.4 eV, respectively, while no satellite peak can be noted on sRM600 due to the formation of Fe<sub>3</sub>O<sub>4</sub> [35]. As shown in Fig. 3b, the [O] can be deconvoluted into three peaks, which are assigned to lattice oxygen (O<sub>α</sub>, 529.9 eV) of Fe<sub>2</sub>O<sub>3</sub>, oxygen vacancy/electrophilic oxygen/lattice oxygen of other metal oxides (O<sub>β</sub>, 531.3 eV), and chemically adsorbed oxygen (O<sub>γ</sub>, 532.5 eV), respectively [36,37]. The content of these oxygen species could be determined based on their peak area ratio and shown in Table 7. The content of O<sub>β</sub> on RM600 is 54.8%, followed by O<sub>α</sub> and O<sub>γ</sub> with the content of 28.0% and 17.2%, respectively. For sRM600, the O<sub>β</sub> is still the main oxygen species, accounting for 63.0%, but the O<sub>α</sub> decreases from 28.0% to 13.5%. The decrease of O<sub>α</sub> is due to the crystal phase transition from Fe<sub>2</sub>O<sub>3</sub> to Fe<sub>3</sub>O<sub>4</sub>.

Raman spectra of RM600 and sRM600 are shown in Fig. 4a. For RM600, bands around 223, 290, 406, 508, 607, 672, and 1325 cm<sup>-1</sup> are attributed to Fe-O bonds. These bands match well with hematite [38], which belongs to the corundum-typed structure (R-3c) crystal space group with two types of Raman-active vibration modes named A<sub>1g</sub> and E<sub>g</sub> [39]. Bands at 223 and 508 cm<sup>-1</sup> are assigned to A<sub>1g</sub> mode, and those of 290, 406, 607 cm<sup>-1</sup> are attributed to the E<sub>g</sub> mode. Band at 672 cm<sup>-1</sup> is related to disorder effect and/or the presence of nanocrystal Fe<sub>2</sub>O<sub>3</sub>, and band at 1325 cm<sup>-1</sup> is associated with hematite two-magnon scattering [38]. No bands attributed to Fe<sub>2</sub>O<sub>3</sub> can be observed on sRM600, and weak bands around 358 and 480 cm<sup>-1</sup> are assigned to the E<sub>g</sub> and T<sub>2g</sub> modes of a typical magnetite Fe<sub>3</sub>O<sub>4</sub> with a cubic inverse spinel phase [40]. A weak band at 358 cm<sup>-1</sup> could be seen when the figure is enlarged. Jiang et al. reported that the band at 358 cm<sup>-1</sup> is also very weak on the Fe<sub>3</sub>O<sub>4</sub> samples [40]. There is a high intensity of G (1600 cm<sup>-1</sup>) and D (1351 cm<sup>-1</sup>) bands, indicating the presence of coke.

H<sub>2</sub>-TPR profiles (Fig. 4b) show that the peak of RM600 is centered at 545 °C. Kim et al. reported that the H<sub>2</sub>-TPR profile of RM is similar with Fe<sub>2</sub>O<sub>3</sub>. Peak at low temperature is related to the reduction from Fe<sub>2</sub>O<sub>3</sub> to Fe<sub>3</sub>O<sub>4</sub>, and peak at high temperature is attributed to further reduction of Fe<sub>3</sub>O<sub>4</sub> to form Fe [41]. These complex reduction reactions can be

**Table 6**

Textural properties of RM samples.

Sample	RM	RM600	sRM600
Specific surface area (m <sup>2</sup> /g)	18.8	30.7	13.0
Pore volume (cm <sup>3</sup> /g)	0.085	0.107	0.059

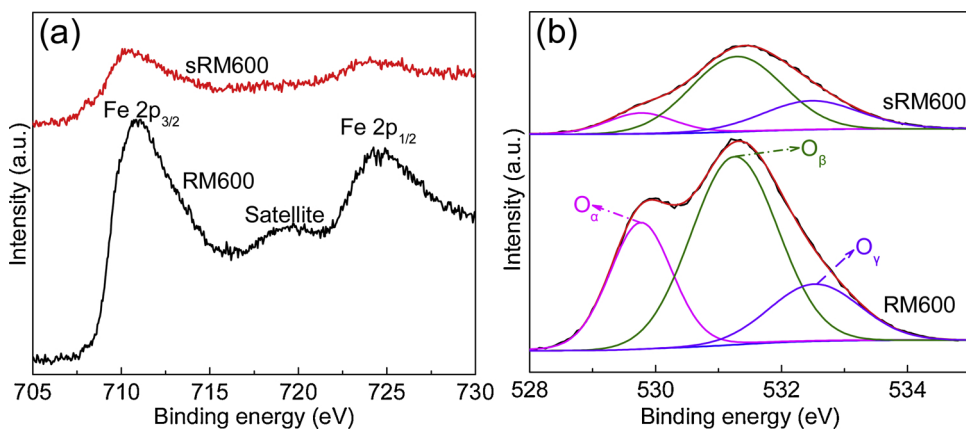
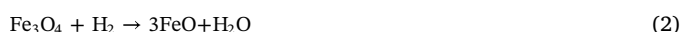


Fig. 3. XPS spectra of Fe 2p (a), and O 1s (b) of RM600 and sRM600.

**Table 7**  
Relative content of active oxygen species on RM600 and sRM600.

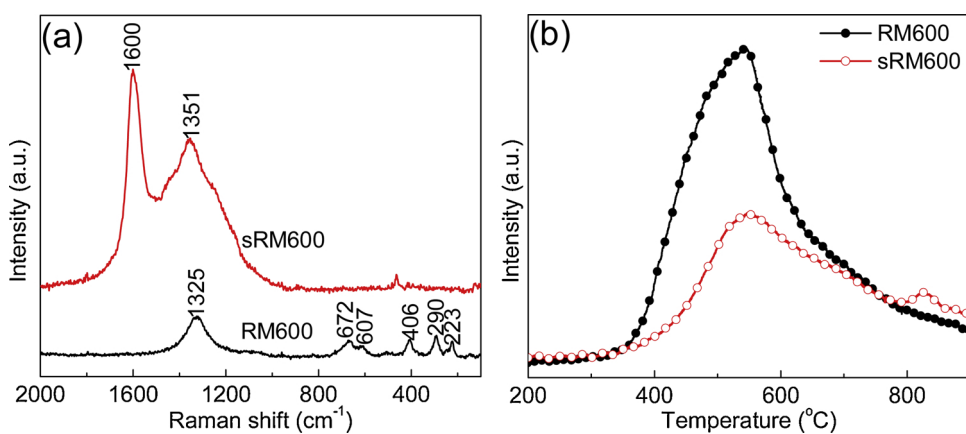
Sample	Relative content of active oxygen species (%)		
	O <sub>α</sub>	O <sub>β</sub>	O <sub>γ</sub>
RM600	28.0	54.8	17.2
sRM600	13.5	63.0	23.5

simply expressed by Eqs. (1)–(3). The reduction peak area of sRM600 is smaller than that of RM600, but the reduction temperature increases from 348 to 384 °C due to the loss of [O]. The reduction of Fe<sub>3</sub>O<sub>4</sub> or FeO requires a high temperature as compared to that of Fe<sub>2</sub>O<sub>3</sub> [41]. Therefore, the reduction peak on sRM600 is mainly assigned to the reduction of Fe<sub>3</sub>O<sub>4</sub> or FeO. It should be noted that the reactions of Eqs. (1)–(3) also occur in the presence of hydrocarbon molecules [14].



The above analysis revealed that Fe<sub>2</sub>O<sub>3</sub> in RM can be considered as an oxidant, which provides [O] to take part in the cracking of VR. Compared to the previous work by using Fe<sub>2</sub>O<sub>3</sub> as oxidant for POX of VR [11,27], the use of RM shows a better performance in terms of gasoline and diesel yields. For example, yields of gasoline and diesel are 8.0 wt% and 27.5 wt% on Fe<sub>2</sub>O<sub>3</sub>, and they increase to 10.3 wt% and 38.0 wt% on RM600, respectively. The EDX elemental mapping (Fig. S5) shows that Fe and O are well dispersed on the RM600 and sRM600, indicating that there is no obvious sintering or agglomeration of the

active sites. As shown in Table 1, the main component in RM is Fe<sub>2</sub>O<sub>3</sub> (39.0 wt%), followed by SiO<sub>2</sub> (22.2 wt%), Al<sub>2</sub>O<sub>3</sub> (21.4 wt%), Na<sub>2</sub>O (11.3 wt%), and TiO<sub>2</sub> (3.6 wt%), respectively. This suggests that better POX performance of RM is not only associated with the presence of Fe<sub>2</sub>O<sub>3</sub>, but also closely related to other components. The presence of other metal oxides or synergism between metal oxides can be contributed to the improved performance. The SiO<sub>2</sub>, Al<sub>2</sub>O<sub>3</sub>, and TiO<sub>2</sub> in RM may give rise to synergistic effect on the overall activity. Bao et al. found that the presence of SiO<sub>2</sub>, Al<sub>2</sub>O<sub>3</sub>, and TiO<sub>2</sub> increases the oxidation and reduction reactivity of RM by developing uniform porous structure inside RM [42]. The positive effect is in the following order of Al<sub>2</sub>O<sub>3</sub> > SiO<sub>2</sub> > TiO<sub>2</sub>. In our previous work, the addition of Al<sub>2</sub>O<sub>3</sub> into Fe<sub>2</sub>O<sub>3</sub> increases the specific surface area and shows a better POX than that of fresh Fe<sub>2</sub>O<sub>3</sub> [11]. The sRM600 shows a specific surface area of 13.0 m<sup>2</sup>/g, which is the same with that of fresh Fe<sub>2</sub>O<sub>3</sub> (13.0 m<sup>2</sup>/g) [11]. The large specific surface area is due to the presence of SiO<sub>2</sub>, Al<sub>2</sub>O<sub>3</sub>, and TiO<sub>2</sub>. Ge et al. reported that the incorporation of Na into Fe<sub>2</sub>O<sub>3</sub> could lead to the formation of sodium ferrite [43], which is an electron donor. The presence of sodium ferrite weakens the Fe-O bond in Fe<sub>2</sub>O<sub>3</sub>. It has been reported that the addition of Na in Fe<sub>2</sub>O<sub>3</sub>/Al<sub>2</sub>O<sub>3</sub> could significantly improve the reduction behavior, thermal stability, and attrition resistance as compared to Fe<sub>2</sub>O<sub>3</sub>/Al<sub>2</sub>O<sub>3</sub> [44]. As shown in Fig. S5, Na is highly distributed on the surface of RM600 before and after reaction. To confirm the change in electron distribution of Fe species, Mössbauer spectra of RM600 was recorded and shown Fig. 5. The spectra of RM600 mainly contains two magnetic sextet spectra related to Fe<sub>2</sub>O<sub>3</sub>, and one as hematite and another is highly dispersed Fe<sup>3+</sup> [32] with content of 46.5% and 39.5%, respectively. One single (Fe<sup>2+</sup>) and doublet (Fe<sup>2.5+</sup>) spectra account for the relative area of 10.7% and 3.3%, respectively. Rochetti Yharour et al. suggested that signals

Fig. 4. Raman spectra (a) and H<sub>2</sub>-TPR profiles (b) of RM600 and sRM600.

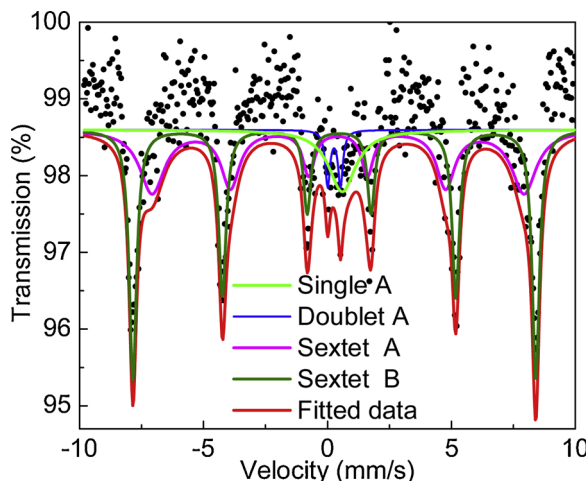


Fig. 5. Room temperature  $^{57}\text{Fe}$  Mössbauer spectra of RM600.



Fig. 6. Possible mechanism of POX of heavy oil over RM.

assigned to  $\text{Fe}^{2+}$  and  $\text{Fe}^{3+}$  can be expressed as  $\text{Fe}^{2.5+}$  [45]. The addition of alkali dopants could result in electron redistribution and microstructure variation of  $\text{Fe}_2\text{O}_3$  and create an “electron deficit” in the doped region [46]. The electron deficit is also known as oxygen vacancy, which could be generated spontaneously to maintain the electrostatic balance [47]. According to the results from Mössbauer spectra analysis, the chemical formula of iron oxide in RM can be expressed as  $\text{Fe}_{2.88}\text{O}_3$ . The stoichiometry of oxygen in  $\text{Fe}_{2.88}\text{O}_3$  is less than the traditional  $\text{Fe}_2\text{O}_3$  due to the presence of oxygen vacancy. It can be concluded that iron oxide in RM is the active sites. The [O] in iron oxide reacts with heavy oil. A better performance of RM can be obtained as compared to the thermal cracking. Metal oxides including  $\text{SiO}_2$ ,  $\text{Al}_2\text{O}_3$ ,

and  $\text{TiO}_2$  increase the thermal stability and inhibit the sintering of particles, therefore, large specific surface area can be remained after reaction. Fe and O are highly dispersed and more [O] could be provided. Na doping weakens the Fe–O bond and creates oxygen vacancy, thus, the [O] in the RM is more active than that in  $\text{Fe}_2\text{O}_3$ . As a result, RM600 exhibits better POX performance than that of  $\text{Fe}_2\text{O}_3$ .

In typical thermal cracking, production of light fuels from heavy oil is based on carbon rejection mechanism with large amount of CR or coke formation [48]. POX of heavy oil also follows carbon rejection mechanism because no extra hydrogen is added into reaction system. However, some differences can be noted because some fraction of carbon in heavy oil are removed by forming  $\text{CO}_2$  or CO [49]. When transition metal oxides are used as an oxidant, the [O] participates into the cleavage of C–C bond [50]. In view of this, transition metal oxides are not as typical catalyst but as reactant. As a result, valence change of metal ions and crystal transition are noted after reaction. When iron oxide based materials are used in heavy oil upgrading, crystal phase transition from hematite ( $\text{Fe}_2\text{O}_3$ ) to magnetite ( $\text{Fe}_3\text{O}_4$ ) can be observed [51]. The possible mechanism involved in POX of heavy oil over RM is illustrated in Fig. 6. The reaction between hydrocarbon molecules and lattice oxygen results in the formation of oxygen-containing intermediates [52], which further undergo decomposition to form alkane and alkene compounds. The lattice oxygen in RM is transferred into the gas phase and exists in the form of CO and  $\text{CO}_2$ . The consumption of lattice oxygen on the surface causes generation of oxygen vacancy. Due to the concentration gradient, the bulk lattice oxygen migrates into the surface to fill the surface oxygen vacancy and the oxygen vacancy moves to the bulk [2]. Finally, more oxygen vacancy are formed as the POX progresses and the rearrangement of Fe atom finally results in crystal phase transition from hematite ( $\text{Fe}_2\text{O}_3$ ) to magnetite ( $\text{Fe}_3\text{O}_4$ ) [53].

### 3.3. Reduction of spent RM

As mentioned above, [O] in  $\text{Fe}_2\text{O}_3$  is consumed and crystal transition from hematite to magnetite structure occurs. Raman analysis of sRM600 confirms the presence of coke. The loss of [O] can be replenished and carbon is burnt off when the sRM600 is heated under air atmosphere. TG analysis was performed and the weight change with respect to temperature was recorded. As shown in Fig. 7a, the weight loss around 100 °C is due to the removal of adsorbed water. The weight increase in the temperature range of 100–350 °C is related to the oxidation of  $\text{Fe}_3\text{O}_4$  in sRM600 to regenerate the consumed [O]. With further increase of temperature, there is an obvious weight loss with 7.7 wt %. The weight loss is mainly attributed to the removal of coke. According to the DTG curve, temperature corresponding to peak of weight loss rate is centered at 400 °C.

XRD and XPS results showed that RM could be in-situ reduced to form  $\text{Fe}_3\text{O}_4$ , and Raman and TG analysis indicated the formation of coke on the sRM600. The formation of  $\text{Fe}_3\text{O}_4$  causes the deactivation of catalyst [7]. How to manage the spent RM is also a key issue for the development of RM utilization. When spent RM is treated under inert

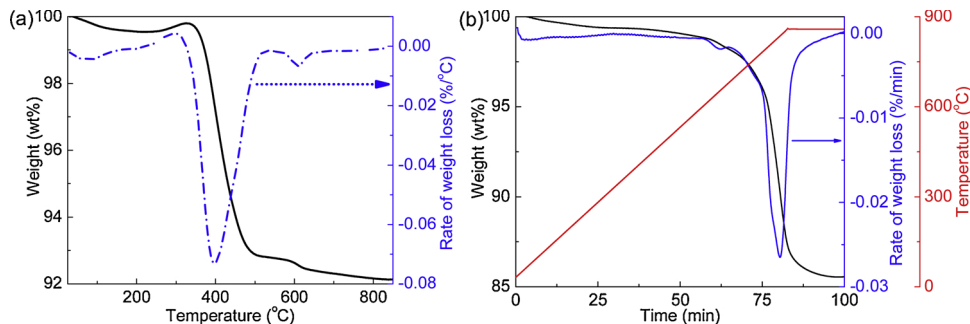


Fig. 7. TG and DTG curves of sRM600 under air (a)  $\text{N}_2$  atmosphere (b).

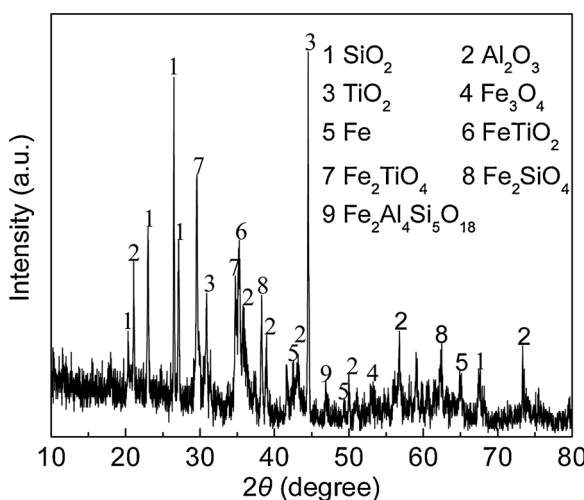


Fig. 8. XRD pattern of RsRM600.

condition, it is possible that  $\text{Fe}_3\text{O}_4$  is reduced by coke to form  $\text{FeO}$  or metallic Fe. To reveal the weight change of this reduction process, TG analysis of the sRM600 was conducted under  $\text{N}_2$  atmosphere. It was heated to from 25 °C to 850 °C with a heating rate of 10 °C/min, and maintained at 850 °C for 20 min. The resulting TG and DTG curves are shown in Fig. 7b. No significant change is observed below 600 °C. The weight loss above 600 °C is attributed to the reduction of  $\text{Fe}_3\text{O}_4$ . According to the DTG curve, peak of weight loss rate is around 820 °C, which suggests that the reduction of  $\text{Fe}_3\text{O}_4$  requires a higher temperature. The final weight loss is 14.5 wt% and possible reactions during this process can be summarized in Eqs. (4) and (5)) [54]:

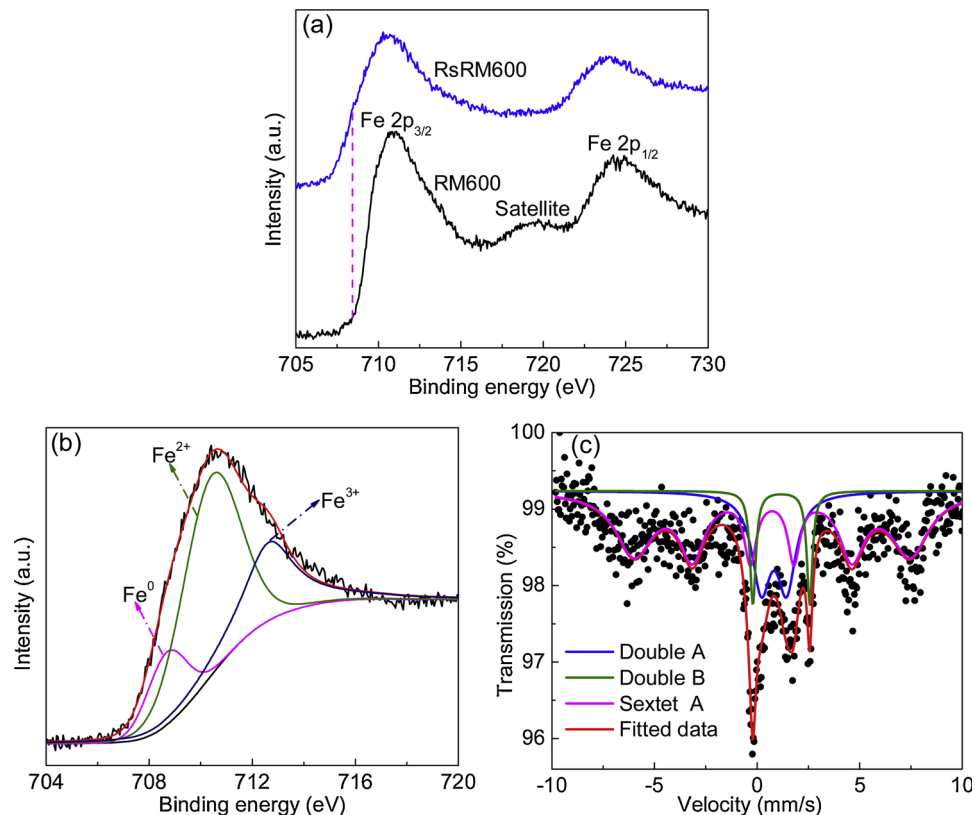


The change in color of sRM600 after reduction (RsRM600) was recorded. After that, RsRM600 was characterized by several techniques, including XRD, SEM, XPS, and room temperature  $^{57}\text{Fe}$  Mössbauer. As shown in Fig. S6, the apparent color of RM600 and sRM600 is reddish-brown and black, respectively. The change in color is mainly due to the formation of magnetite ( $\text{Fe}_3\text{O}_4$ ) and coke deposition, both of which are in color of black. For RsRM600, its color changes to gray as shown in Fig. S6(c).

Fig. 8 shows the XRD pattern of RsRM600. Peaks attributed to  $\text{SiO}_2$  and  $\text{Al}_2\text{O}_3$  can still be observed. New diffraction peaks at 42.5°, 49.3°, and 65.0° are assigned to metallic Fe. This suggests that  $\text{Fe}_3\text{O}_4$  is reduced by coke to form  $\text{FeO}$  and then Fe. The other new diffraction peaks are mainly assigned to  $\text{FeTiO}_2$ ,  $\text{Fe}_2\text{TiO}_4$ ,  $\text{Fe}_2\text{SiO}_4$  and  $\text{Fe}_2\text{Al}_4\text{Si}_5\text{O}_{18}$ . When  $\text{Fe}_3\text{O}_4$  is reduced to  $\text{FeO}$ ,  $\text{TiO}_2$ ,  $\text{Al}_2\text{O}_3$ , and  $\text{SiO}_2$  in RM will react with  $\text{FeO}$  to form  $\text{FeTiO}_2$ ,  $\text{Fe}_2\text{TiO}_4$ ,  $\text{Fe}_2\text{SiO}_4$  and  $\text{Fe}_2\text{Al}_4\text{Si}_5\text{O}_{18}$ .

As shown in Fig. S7, the morphology of RM600 is irregular, partial size is relatively uniform, and some large particles can be observed. The particle size of RsRM600 is larger than that of RM600. This indicates that severe agglomeration and sintering occur during reduction process. The specific surface area and pore volume on RM600 are  $30.7 \text{ m}^2/\text{g}$  and  $0.107 \text{ cm}^3/\text{g}$ , but they decrease to  $5.9 \text{ m}^2/\text{g}$  and  $0.041 \text{ cm}^3/\text{g}$ , respectively, on RsRM600. The decrease of specific surface area and pore volume is due to the sintering of particles and collapse of pore structure.

As shown in Fig. 9a, there is no satellite peak on RsRM600, and peaks of  $\text{Fe } 2p_{3/2}$  and  $\text{Fe } 2p_{1/2}$  shift to a lower binding energy. Three different states of iron species including  $\text{Fe}^{3+}$ ,  $\text{Fe}^{2+}$ , and  $\text{Fe}^0$  are on RsRM600. To determine relative content of these iron species, the  $\text{Fe } 2p_{3/2}$  peak is fitted into three peaks as shown in Fig. 9b, and the relative percentage is determined based on peak area ratio. The relative content of  $\text{Fe}^0$ ,  $\text{Fe}^{2+}$ , and  $\text{Fe}^{3+}$  on RsRM600 is 28.8%, 57.5%, and 13.7%, respectively. The room temperature  $^{57}\text{Fe}$  Mössbauer spectra of RsRM600 could be fitted with two doubles and one sextet (Fig. 9c). The double A,

Fig. 9. Detail XPS spectra of Fe 2p (a), deconvolution of Fe 2p<sub>3/2</sub> (b), and room temperature  $^{57}\text{Fe}$  Mössbauer (c) of RsRM600.

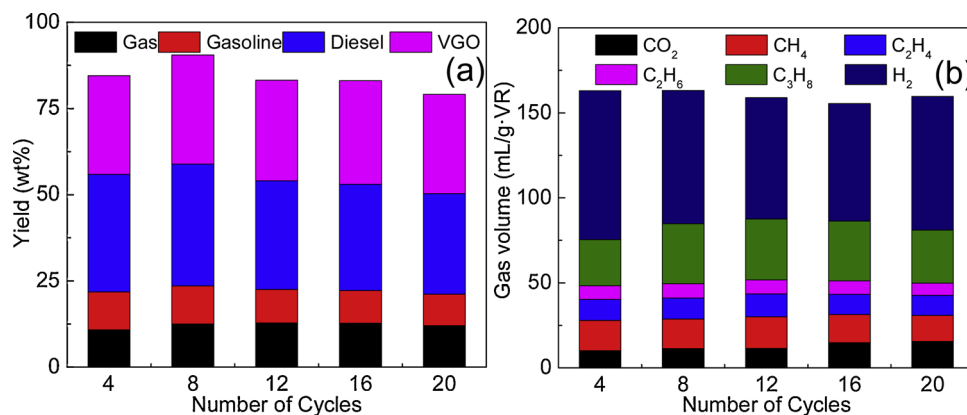


Fig. 10. Yields of gas, gasoline, diesel and VGO (a) and composition of gas (b) over RM600 after 20 cycles.

B and sextet spectrum are related to Fe<sup>0</sup>, Fe<sup>3+</sup>, and Fe<sup>2+</sup> with relative content of 24.2%, 9.4% and 66.4%, respectively, which is consistent with the XPS analysis. The above results show that coke can be used as reducing agent to reduce Fe<sub>3</sub>O<sub>4</sub> in RM. It provides a new method for recovering valuable metallic Fe from RM.

#### 3.4. Chemical looping partial oxidation of VR

The magnetite (Fe<sub>3</sub>O<sub>4</sub>) is formed on the spent RM. It has been reported that the formation of Fe<sub>3</sub>O<sub>4</sub> will cause the deactivation of catalyst [7]. The regenerability of RM600 was conducted at the same reactor by switching the carrier gas N<sub>2</sub> to air. Coke is burnt off and the loss of oxygen can be replenished when it was treated in air at 550 °C. The regeneration step was believed to be finished when no CO<sub>2</sub> was detected and the gas composition in the exhaust was the same as air. The above process forms a CLPOX cycle. The gas, gasoline, diesel and VGO yields with 20 cycles is shown in Fig. 10. Generally, the yield of these products remains stable with the increase of cycle. As shown in Fig. 10a, the gas, gasoline, diesel and VGO yields at 4<sup>th</sup> cycle are 10.8, 11.0, 34.1, and 28.6 wt%, and they are 12.0, 9.1, 29.2 and 28.8 wt% at 20<sup>th</sup> cycle, respectively. CO<sub>2</sub> is a by-product of POX. Fig. 10b shows that the CO<sub>2</sub> yield keeps stable with the increase of cycle due to the effective regeneration of [O]. It can be seen that the H<sub>2</sub> yield decreases slightly at the initial cycles, but it keeps constant with the further increase of cycle. For example, the H<sub>2</sub> yield is 88 mL/g·VR at 4<sup>th</sup> cycle, and it is 79 mL/g·VR at 20<sup>th</sup> cycle. The obtained results show that RM600 has a good regenerability and is a good oxygen carrier for the CLPOX process.

#### 4. Conclusion

Integrated process of POX of heavy oil and in-situ reduction of Fe<sub>2</sub>O<sub>3</sub> in RM was investigated, and the role of diverse metal oxides in RM on the high POX performance was clarified. The use of coke as reducing agent and CLPOX processes were proposed. It is shown that the addition of RM600 contributes to the deep conversion of heavy oil and decreases cracking temperature. The yields of gasoline and diesel on RM600 are 10.3 wt% and 38.0 wt%, respectively. The resulting liquid product is rich in straight-chain alkane and alkene compounds. Fe<sub>2</sub>O<sub>3</sub> in RM is in-situ reduced by VR to form Fe<sub>3</sub>O<sub>4</sub>. The transition from Fe<sub>2</sub>O<sub>3</sub> to Fe<sub>3</sub>O<sub>4</sub> shows that Fe<sub>2</sub>O<sub>3</sub> is the active site, providing [O] to participate in the reaction. Large specific surface area is remained after reaction due to the presence of Al<sub>2</sub>O<sub>3</sub>, SiO<sub>2</sub>, and TiO<sub>2</sub>. The presence of Na species forms sodium ferrite, which weakens Fe-O bond and creates more oxygen vacancy. Fe<sub>3</sub>O<sub>4</sub> in spent RM can be reduced by coke with the formation of metallic Fe. The CLPOX by using RM600 as oxygen carrier shows good regenerability during 20 cycles. The yields of gas, gasoline, diesel, and VGO at 20<sup>th</sup> cycle are 12.0 9.1, 29.2 and 28.8 wt%, respectively.

#### Declaration of Competing Interest

None.

#### Acknowledgements

This work was supported by the Joint Fund of Coal-based Low Hydrocarbons by NSFC and Shanxi Provincial Government of China (No. U1710105), Research Fund of the State Key Laboratory of Fine Chemistry (No. ZYTS201804) in Dalian University of Technology, National Natural Science Foundation of China (No. 21776039), and National Natural Science Foundation of China Youth Science Fund Project (No.51306028).

#### Appendix A. Supplementary data

Supplementary material related to this article can be found, in the online version, at doi:<https://doi.org/10.1016/j.apcatb.2019.117944>.

#### References

- [1] Y. Zhang, L. Huang, X. Xi, W. Li, G. Sun, S. Gao, S. Zhang, Energy Fuel 31 (2017) 9915–9922.
- [2] H.S. Lim, M. Lee, D. Kang, J.W. Lee, Int. J. Hydrogen Energy 43 (2018) 20580–20590.
- [3] H.S. Lim, D. Kang, J.W. Lee, Appl. Catal. B 202 (2017) 175–183.
- [4] C. Nguyen-Huy, E.W. Shin, Fuel 192 (2017) 149–157.
- [5] D. Wang, L. Jin, Y. Li, H. Hu, Energy Fuel 33 (2019) 257–265.
- [6] C. Nguyen-Huy, E.W. Shin, Fuel 179 (2016) 17–24.
- [7] H.S. Lee, C. Nguyen-Huy, T. Pham, E.W. Shin, Fuel 165 (2016) 462–467.
- [8] V.F. Shvets, V.N. Sapunov, R.A. Kozlovskiy, A.I. Luganskiy, A.V. Gorbulov, F.S. Sovetin, T.N. Gartman, Chem. Eng. J. 329 (2017) 275–282.
- [9] J. Liu, Y. Xing, Y. Chen, P. Yuan, Z. Cheng, W. Yuan, Ind. Eng. Chem. Res. 57 (2018) 867–875.
- [10] C. Li, Y. Chen, J. Hou, C. Zhou, Fuel 214 (2018) 123–126.
- [11] D. Wang, L. Jin, Y. Li, H. Hu, Fuel 210 (2017) 803–810.
- [12] J. Hu, V. Galvita, H. Poelman, G. Marin, Mater. 11 (2018) 1187.
- [13] H. Jahromi, F.A. Agblevor, Ind. Eng. Chem. Res. 57 (2018) 13257–13268.
- [14] G. Deng, K. Li, Z. Gu, X. Zhu, Y. Wei, X. Cheng, H. Wang, Chem. Eng. J. 341 (2018) 588–600.
- [15] A. Castille, C. Bessette, F. Thomas, M. Etemad, Catal. Commun. 121 (2019) 5–10.
- [16] H. Jahromi, F.A. Agblevor, Appl. Catal. A 558 (2018) 109–121.
- [17] S. Sushil, V.S. Batra, Appl. Catal. B 81 (2008) 64–77.
- [18] H. Jahromi, F.A. Agblevor, Appl. Catal. B 236 (2018) 1–12.
- [19] F.A. Agblevor, D.C. Elliott, D.M. Santosa, M.V. Olarte, S.D. Burton, M. Swita, S.H. Beis, K. Christian, B. Sargent, Energy Fuel 30 (2016) 7947–7958.
- [20] J. Weber, A. Thompson, J. Wilmoth, V.S. Batra, N. Janulaitis, J.R. Kastner, Appl. Catal. B 241 (2019) 430–441.
- [21] F.G. Mendonça, J.P.M. Gomes, J.C. Tristão, J.D. Ardisson, R.R. Soares, R.M. Lago, Fuel 184 (2016) 36–41.
- [22] A. López, I. de Marco, B.M. Caballero, M.F. Laresgoiti, A. Adrados, A. Aranzabal, Appl. Catal. B 104 (2011) 211–219.
- [23] O.A. Omoniyi, V. Dupont, Appl. Catal. B 242 (2019) 397–409.
- [24] S. Yusuf, V. Haribal, D. Jackson, L. Neal, F. Li, Appl. Catal. B 257 (2019) 117885.
- [25] J. Hu, V.V. Galvita, H. Poelman, C. Detavernier, G.B. Marin, Appl. Catal. B 231 (2018) 123–136.
- [26] L. Qin, M. Guo, Y. Liu, Z. Cheng, J.A. Fan, L. Fan, Appl. Catal. B 235 (2018)

143–149.

- [27] D. Wang, L. Jin, Y. Li, B. Wei, D. Yao, H. Hu, *Fuel* 239 (2019) 764–773.
- [28] J. Hao, Y. Che, Y. Tian, D. Li, J. Zhang, Y. Qiao, *Energy Fuel* 31 (2017) 1295–1309.
- [29] S. Ebrahimi, J.S. Moghaddas, M.K.R. Aghjeh, *Fuel* 87 (2008) 1623–1627.
- [30] Y. Che, J. Hao, J. Zhang, Y. Qiao, D. Li, Y. Tian, *Energy Fuel* 32 (2018) 1348–1357.
- [31] B. Tian, Y. Qiao, L. Bai, W. Feng, Y. Jiang, Y. Tian, *Energy Convers. Manage.* 140 (2017) 109–120.
- [32] A.A.S. Oliveira, D.A.S. Costa, I.F. Teixeira, F.C.C. Moura, *Appl. Catal. B* 162 (2015) 475–482.
- [33] T. Radu, C. Iacobita, D. Benea, R. Turcu, *Appl. Surf. Sci.* 405 (2017) 337–343.
- [34] W. Zhu, T. Zhang, Y. Zhang, Z. Yue, Y. Li, R. Wang, Y. Ji, X. Sun, J. Wang, *Appl. Catal. B* 244 (2019) 844–852.
- [35] M. Mühlner, R. Schlögl, G. Ertl, *J. Catal.* 138 (1992) 413–444.
- [36] X. Wu, Y. Zhang, X. Dou, B. Zhao, M. Yang, *Chem. Eng. J.* 223 (2013) 364–370.
- [37] Q. Si, Q. Zhu, Z. Xing, *ACS Sustain. Chem. Eng.* 5 (2017) 11422–11432.
- [38] D. Trpkov, M. Panjan, L. Kopanja, M. Tadić, *Appl. Surf. Sci.* 457 (2018) 427–438.
- [39] L. Li, X. She, J. Yi, L. Pan, K. Xia, W. Wei, X. Zhu, Z. Chen, H. Xu, H. Li, *Appl. Surf. Sci.* 469 (2019) 933–940.
- [40] F. Jiang, X. Wang, D. Wu, *Appl. Energy* 134 (2014) 456–468.
- [41] S.C. Kim, S.W. Nahm, Y. Park, *J. Hazard. Mater.* 300 (2015) 104–113.
- [42] J. Bao, L. Chen, F. Liu, Z. Fan, H.S. Nikolic, K. Liu, *Ind. Eng. Chem. Res.* 55 (2016) 8046–8057.
- [43] H. Ge, L. Shen, H. Gu, T. Song, S. Jiang, *Fuel* 159 (2015) 107–117.
- [44] W. Huang, Y. Kuo, P. Su, Y. Tseng, H. Lee, Y. Ku, *Chem. Eng. J.* 334 (2018) 2079–2087.
- [45] M.F. Rochetti Yharour, N.A. Fellenz, A.M. Alvarez, J.F. Bengoa, N.G. Gallegos, M.V. Cagnoli, S.G. Marchetti, *Int. J. Hydrogen Energy* 39 (2014) 12563–12571.
- [46] Y. Feng, N. Wang, X. Guo, *Fuel* 236 (2019) 1057–1064.
- [47] E.W. McFarland, H. Metiu, *Chem. Rev.* 113 (2013) 4391–4427.
- [48] M.S. Rana, V. Sámano, J. Ancheyta, J.A.I. Diaz, *Fuel* 86 (2007) 1216–1231.
- [49] D. Wang, L. Jin, Y. Li, D. Yao, J. Wang, H. Hu, *Energy* 162 (2018) 542–553.
- [50] M. Hosseinpour, S. Fatemi, S.J. Ahmadi, *Fuel* 159 (2015) 538–549.
- [51] M. Hosseinpour, S. Fatemi, S.J. Ahmadi, M. Morimoto, M. Akizuki, Y. Oshima, E. Fumoto, *Appl. Catal. B* 230 (2018) 91–101.
- [52] M. Hosseinpour, S. Fatemi, S.J. Ahmadi, *J. Supercrit. Fluid.* 110 (2016) 75–82.
- [53] C. Dong, S. Sheng, W. Qin, Q. Lu, Y. Zhao, X. Wang, J. Zhang, *Appl. Surf. Sci.* 257 (2011) 8647–8652.
- [54] S. Hosokai, K. Matsui, N. Okinaka, K. Ohno, M. Shimizu, T. Akiyama, *Energy Fuel* 26 (2012) 7274–7279.